applied sciences

MDPI

Article

Improved ADRC-Based Autonomous Vehicle Path-Tracking Control Study Considering Lateral Stability

Nan Kang, Yi Han *, Tian Guan and Siyu Wang

School of Automobile, Chang'an University, Xi'an 710064, China; 2021022008@chd.edu.cn (N.K.); 2021022006@chd.edu.cn (T.G.); 2021122002@chd.edu.cn (S.W.)
* Correspondence: hany@chd.edu.cn; Tel.: +86-132-2805-5890

Abstract: The antidisturbance control problem of autonomous vehicle path tracking considering lateral stability is studied in this paper. This paper proposes an improved active disturbance rejection control (IADRC) control method including an improved extended state observer (IESO) and an error compensator based on LQR, where a new continuous nonlinear function is proposed in the IESO instead of the classical piecewise function. Based on the IADRC, an autonomous vehicle path-tracking controller considering lateral stability is designed. Using the output wheel steering angle and external yaw moment, the IESO estimates the disturbance value and compensates for the disturbance in the feedback to meet the goal of antidisturbance control. Based on the concept of control allocation (CA), the control distributor is designed to distribute the external yaw moment to the four wheels in a reasonable and optimal way to achieve differential braking. Finally, the control scheme is evaluated in the form of CarSim/Simulink cosimulation; the results show that the proposed autonomous vehicle path-tracking control scheme has better path-tracking effect and higher antidisturbance robustness.

Keywords: autonomous vehicle; path tracking; improved active disturbance rejection control; lateral stability

Citation: Kang, N.; Han, Y.; Guan, T.; Wang, S. Improved ADRC-Based Autonomous Vehicle Path-Tracking Control Study Considering Lateral Stability. *Appl. Sci.* **2022**, *12*, 4660. https://doi.org/10.3390/app12094660

Academic Editors: Jian Zhang and Konstantinos Gkoumas

Received: 7 March 2022
Accepted: 29 April 2022
Published: 6 May 2022

Publisher's Note: MDPI stays neutral with regard to jurisdictional claims in published maps and institutional affiliations.

1. Introduction

In recent decades, with the development of society, cars have become one of the necessary means of transportation for people's daily travel, and autonomous vehicle have received wide attention from the society by virtue of their advantages in improving road traffic safety and reducing road traffic congestion [1]. Many countries worldwide are strengthening research in areas such as autonomous vehicle, and autonomous vehicle technology has become one of the key points and hot spots of research in the automotive industry at present [2]. Meanwhile, owing to the leapfrog development of the electronic industry and control technology, autonomous vehicle technology has also made great progress [3,4]. Autonomous vehicle technology mainly includes three parts: environment perception, path planning, and tracking control, among which path-tracking control is the research content of this paper. Path-tracking control is to achieve the desired path given by the path planning part by controlling wheel steering, and its control effect directly affects the performance and safety stability of autonomous vehicle [5]. Because of the complexity of vehicle driving conditions, it will be affected by various disturbances, and how to achieve the suppression of disturbances plays a crucial role in the autonomous vehicle path-tracking control accuracy and safety.

As one of the key technologies for autonomous vehicle, path-tracking control is to eliminate the tracking deviation generated between the actual driving path and the desired path during the vehicle driving process by controlling the front-wheel steering or four-wheel steering, so that the autonomous vehicle's driving path tracks the desired path [6,7]. In recent research literature, many various path-tracking control algorithms have been proposed: [8,9] proposed a model predictive control (MPC)-based autonomous vehicle

path-tracking control scheme by constraining the front-wheel steering angle to control the autonomous vehicle along the desired path by front-wheel steering. In [10], two sliding-mode controllers were used to converge the lateral deviation and heading error of the vehicle to zero by four-wheel steering, so that the vehicle travels along the desired path. The results show that the control method using wheel steering has better path-tracking control effect; however, the lateral stability of the vehicle is affected when the lateral force of the tires tends to saturate under large lateral acceleration. Therefore, Hu [11], Chen [12], Hang [13], and other scholars [14–17] have fully considered the lateral stability of the vehicle while focusing on the path-tracking control effect of the autonomous vehicle. In [11–14], the yaw stability problem is considered and the control method of direct yaw moment control (DYC) is used. The controllers described in the literature generate external yaw moments to improve the yaw stability so that the yaw rate of the vehicle tracks the desired value, thus achieving the purpose of improving the vehicle yaw stability. For the implementation of the external yaw moment, the method of optimal distribution of tire forces is used in [12,13], and the method of individual wheel selection rules is used in [14]. Other studies [15,16] consider the problem of the vehicle's roll stability and design an antiroll controller in the autonomous vehicle's path-tracking process, so that the vehicle has both higher path-tracking accuracy and better antiroll stability, which improves the lateral stability of the vehicle. In [17], yaw stability and roll stability are both considered; an integrated controller is designed using sliding-mode control method to comprehensively improve the lateral stability of the autonomous vehicle during path tracking.

By summary and analysis, autonomous vehicle path-tracking control schemes designed in the literature reported above need to be based on accurate models of vehicle dynamics or accurate related parameters; however, there are always simplified parts in models or parameter uncertainties, and external disturbances in autonomous vehicle systems, etc.; these factors may lead to the robustness of the control system that is affected. Therefore, Hiraoka [18] focused on the uncertainty of the system and designed a path-tracking controller based on the sliding-mode control method; the results showed that the controller has robust capability against system uncertainties. As is well known in the antidisturbance problem, active disturbance rejection control (ADRC) has received much attention and application because of its advantage of being able to estimate the disturbance value and compensate for the disturbance in the feedback. Sang [19], Suhail [20], Xia [21], and other scholars [22] designed autonomous vehicle path-tracking control systems based on ADRC; the results show that the controllers have strong robustness against parameter uncertainty and external disturbance. Among them, [19] adopts the ADRC control method; [20] adopts the control method of combined MPC and ADRC; [21] adopts the method of combined differential flatness and ADRC; the method of combined linear active disturbance rejection control (LADRC) and quantitative feedback theory is adopted in [22]. However, it can be seen that the nonlinear functions used in ADRC are piecewise functions and do not have continuity, which may lead to jittering of the control input, which is the focus of this paper.

In summary, this paper focuses on the autonomous vehicle path-tracking control problem considering lateral stability based on the IADRC method, proposes an IADRC control scheme for the problems such as complexity of ADRC parameter tuning and control input jittering phenomenon. The control scheme uses a novel nonlinear function with continuity to solve the problem of control input jittering; the linear quadratic regulator (LQR) control method is used as the error compensator in the classic ADRC, so that the parameters to be tuned in the error compensator have a clear physical meaning and the parameter tuning process is optimized. To improve the lateral stability of the vehicle, a DYC controller is designed to output an external yaw moment. A control distributor is designed based on the concept of control allocation (CA) by means of differential braking to distribute the external yaw moment to the four wheels in a reasonable and optimal way. Finally, the control scheme is evaluated in the form of a CarSim/Simulink cosimulation. The main contributions of this paper include the following:

(1) An IADRC method is proposed in which a new continuous nonlinear function is proposed to replace the classic piecewise function.
(2) An autonomous vehicle path-tracking control scheme is proposed based on the IADRC; the control system can estimate the real-time action value of the parameter uncertainty and disturbance, and then compensation in the feedback realizes the antidisturbance capability of the controller and improves the robustness of the control system against parameter uncertainty and external disturbance.
(3) Using the CA concept, a control distributor is designed to optimize and coordinate of each wheel in real-time; the external yaw moment used to improve the lateral stability of the vehicle is realized in the form of differential braking.

The structure of the rest of this paper is shown as follows. In Section 2, the vehicle model including dynamics and path-tracking components are built for the purpose of control system design, followed by an improved ADRC method, which is introduced in Section 3. In Section 4, an autonomous vehicle path-tracking controller is designed, and the effectiveness of the control scheme is verified in Section 5, followed by a comprehensive conclusion in Section 6.

2. Vehicle Model

2.1. Vehicle Dynamics Model

The two degrees of freedom (2-DOF) linear vehicle model is the basis for designing a control system. Based on the research content of this paper, ignoring the motion degrees of freedom such as vertical, roll, and pitch, and assuming that the suspension system is rigidly connected, the wheel characteristics of the left and right sides of the vehicle are the same. Therefore, we have a 2-DOF vehicle model that includes lateral motion degrees of freedom and yaw motion degrees of freedom. The simplified model is shown in Figure 1a, and the origin of the coordinate system is fixed at the center of mass of the vehicle, the x-axis indicates the longitudinal motion, the longitudinal velocity is considered as a constant value, and the y-axis indicates the lateral motion. The symbols L_1, L_2, R_1, and R_2 of the wheels correspond to the front-left, the rear-left, the front-right, and the rear-right, respectively.

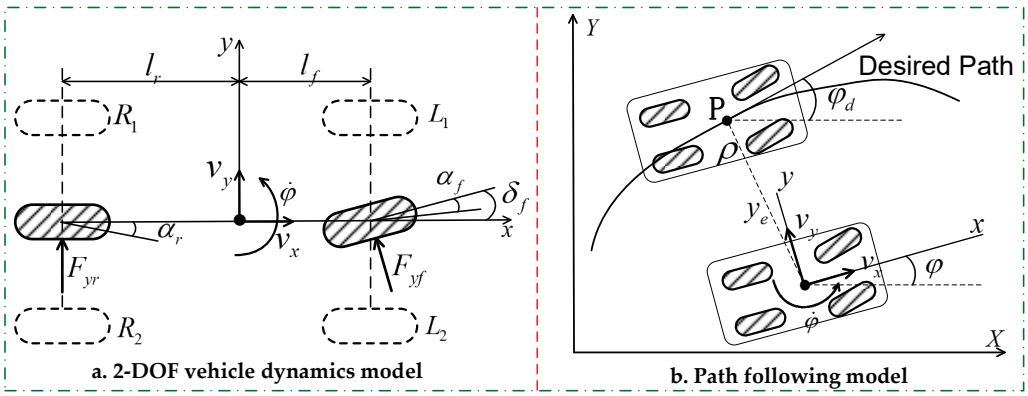

Figure 1. Vehicle model.

By small angle assumptions, the lateral and yaw equations of motion for the 2-DOF vehicle dynamics model are expressed as

$$\begin{cases} m(\ddot{y} + v_x\dot{\varphi}) = F_{yf} + F_{yr} \\ I_z\ddot{\varphi} = l_f F_{yf} - l_r F_{yr} + \Delta M_z \end{cases} \quad (1)$$

where m is the vehicle's total mass, I_z is the yaw moment of inertia; v_x is the longitudinal velocity; y represents lateral displacement, φ is heading angle; l_f, l_r are the distances from the front and rear axles to the center of gravity, respectively; ΔM_z is the active external yaw

moment; F_{yf} is lateral force on the front axle; and F_{yr} is lateral force on the rear axle. F_{yf} and F_{yr} can be defined as

$$\begin{cases} F_{yf} = 2C_f\alpha_f \\ F_{yr} = 2C_r\alpha_r \end{cases} \tag{2}$$

where C_f, C_r are expressed as the linear cornering stiffness; α_f, α_r are the slip angles of the front and rear tires, respectively, which can be defined as

$$\begin{cases} \alpha_f = \delta_f - \frac{v_y + l_f\dot{\varphi}}{v_x} \\ \alpha_r = \frac{l_r\dot{\varphi} - v_y}{v_x} \end{cases} \tag{3}$$

where δ_f is expressed as the front-wheel steering angle.

By associating Equations (1)–(3), we can derive the dynamics model of a 2-DOF vehicle system as follows:

$$\begin{cases} \ddot{y} = \frac{2C_f}{m}\left(\delta_f - \frac{v_y + l_f\dot{\varphi}}{v_x}\right) + \frac{2C_r}{m}\frac{l_r\dot{\varphi} - v_y}{v_x} - v_x\dot{\varphi} \\ \ddot{\varphi} = \frac{1}{I_z}\left[2C_f l_f\left(\delta_f - \frac{v_y + l_f\dot{\varphi}}{v_x}\right) - 2C_r l_r\frac{l_r\dot{\varphi} - v_y}{v_x} + \Delta M_z\right] \end{cases} \tag{4}$$

2.2. Vehicle Path-Tracking Model

Autonomous vehicle path tracking is to control the vehicle wheels to actively steer along the desired path, so as to achieve the purpose of automatic driving. How to eliminate the tracking deviation of lateral displacement and heading angle is the fundamental problem of designing the controller. Selecting the lateral deviation and heading error as the evaluation index of the path-tracking effect, the path-tracking model is established, as shown in Figure 1b, where the X and Y axis represent the longitudinal and horizontal axis of the geodetic coordinate system, respectively; φ_d indicates the desired heading angle; y_e represents the tracking deviation of lateral displacement, which can be used as the path-tracking performance evaluation index; and ρ represents the radius of curvature of the desired path.

The tracking deviation of heading angle and its derivative can be defined as

$$\begin{cases} \varphi_e = \varphi - \varphi_d \\ \dot{\varphi}_e = \dot{\varphi} - \dot{\varphi}_d \end{cases} \tag{5}$$

where φ_e indicates the heading error and $\dot{\varphi}_d$ is the derivative of desired heading angle, and can be expressed as

$$\dot{\varphi}_d = \frac{v_x}{\rho} \tag{6}$$

By using the Serret–Frenet equation and assuming that the heading angle is relatively small, the tracking deviation of lateral displacement can be simplified as

$$\dot{y}_e = v_y + v_x\varphi_e \tag{7}$$

Combining Equations (4)–(6) and substituting into Equation (7), we can derive the vehicle path-tracking model as follows:

$$\frac{d}{dt}x = A_1x + B_1u + E_1\frac{1}{\rho} \tag{8}$$

where $A_1 = \begin{bmatrix} 0 & 1 & 0 & 0 \\ 0 & -2\frac{C_f+C_r}{mv_x} & 2\frac{C_f+C_r}{m} & 2\frac{-l_fC_f+l_rC_r}{mv_x} \\ 0 & 0 & 0 & 1 \\ 0 & 2\frac{-l_fC_f+l_rC_r}{I_zv_x} & 2\frac{l_fC_f-l_rC_r}{I_z} & -2\frac{l_f^2C_f+l_r^2C_r}{I_zv_x} \end{bmatrix}$, $B_1 = \begin{bmatrix} 0 & 0 \\ 2\frac{C_f}{m} & 0 \\ 0 & 0 \\ 2\frac{l_fC_f}{I_z} & \frac{1}{I_z} \end{bmatrix}$,

$E_1 = \begin{bmatrix} 0 \\ 2\frac{-l_fC_f+l_rC_r}{m} - v_x^2 \\ 0 \\ -2\frac{l_f^2C_f+l_r^2C_r}{I_z} \end{bmatrix}$, $x = \begin{pmatrix} y_e & \dot{y}_e & \varphi_e & \dot{\varphi}_e \end{pmatrix}^T$, $u = \begin{pmatrix} \delta_f & \Delta M_z \end{pmatrix}^T$.

3. Improved ADRC

The core idea of ADRC proposed by Han is to treat the disturbance imposed on the system as an extended state variable and design an extended state observer (ESO) to estimate the disturbance and give compensation in the feedback to eliminate the effect of disturbance, so that the ADRC can obtain robustness against the disturbance [23,24]. However, the nonlinear function named fal in ADRC is a piecewise function, and the derivatives of the function are not continuous at the piecewise points. According to the experiment and analysis, the fal function may cause jittering in the disturbance estimation, leading to further jittering in the control input variable. To solve the problem, this paper proposes a new continuous nonlinear function whose derivative is also a continuous function. In order to optimize the parameter tuning process, the LQR control method is used as the error compensator in the ADRC, and the parameters to be tuned in the LQR controller have physical meaning, which simplifies the parameter tuning process. In this way, we obtain the IADRC, as shown in Figure 2.

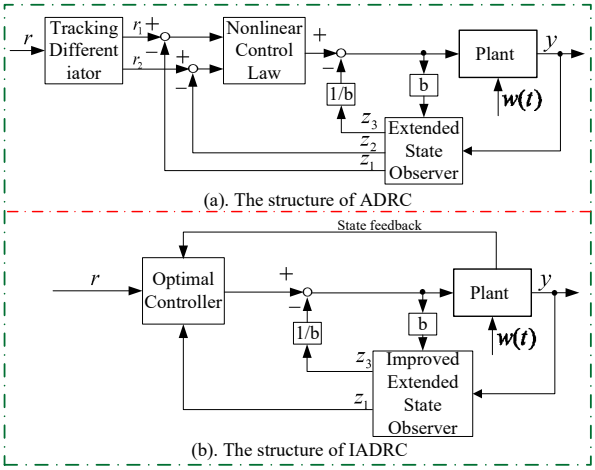

Figure 2. The structure of IADRC.

3.1. Classic ESO Analysis and Improvement

Antidisturbance capability is the core performance of ADRC, which is achieved by estimating the real-time action value of disturbance internal and external in the system through the ESO and giving compensation in the feedback to eliminate the effect of disturbance.

According to the actual problem that is the subject this paper, a single input and single output system is discussed below, assuming that a second-order system is represented as follows [23,24]:

$$\begin{cases} \dot{x}_1 = x_2 \\ \dot{x}_2 = f(\cdot) + bu \\ y = x_1 \end{cases} \tag{9}$$

where $f(\cdot)$ is the total disturbance of the system, which can be seen as an extended state variable represented by x_3.

Therefore, according to the ADRC control theory, we can obtain the extended system:

$$\begin{cases} \dot{x}_1 = x_2 \\ \dot{x}_2 = x_3 + bu \\ \dot{x}_3 = \dot{f}(\cdot) \\ y = x_1 \end{cases} \tag{10}$$

Assuming that the estimated value of the extended state variables are $Z = [z_1, z_2, z_3]^T$, the extended state observer is constructed according to Equation (10), as shown in Equation (11), so that we can estimate the total unknown disturbance, that is, $f(\cdot) = z_3$. Therefore, the nonlinear ESO can be expressed as

$$\begin{cases} e = z_1 - y \\ \dot{z}_1 = z_2 - \beta_{01} e \\ \dot{z}_2 = z_3 - \beta_{02} fal(e, a_1) + bu \\ \dot{z}_3 = -\beta_{03} fal(e, a_2) \end{cases} \tag{11}$$

where β_{01}, β_{02}, β_{03} are the observer gains in the ESO, respectively, and fal is the function used to implement the ESO nonlinearity, and can be expressed as

$$fal(e, a_i, \delta) = \begin{cases} \frac{e}{\delta^{1-a_i}}, & |e| \le \delta \\ |e|^{a_i} \mathrm{sgn}(e), & |e| > \delta \end{cases} \tag{12}$$

where $i = 1, 2$, a_i, δ represent the piecewise function parameters.

In this function, the magnitude of a determines the degree of nonlinearity of the function; the larger the value of a, the stronger the degree of linearity of the function, and vice versa, the weaker the degree of nonlinearity. Parameter δ is the piecewise point of the piecewise function, which determines the length of the linear interval. In the process of control system design, the selection of the value for δ is important, and may lead to the jitter phenomenon of disturbance estimation, which further leads to jitter in the control input signal.

The function in Equation (12) is an odd function symmetric about the origin, so it may be useful to analyze the situation when e > 0, and the same situation when e < 0. The derivative of the function at the piecewise point δ is obtained as

$$fal'(e, a_i, \delta) = \begin{cases} \delta^{a_i - 1}, & 0 < \mathrm{e} \le \delta \\ a_i e^{a_i - 1}, & \mathrm{e} > \delta \end{cases} \tag{13}$$

when e $=\delta$, then $a_i e^{a_i - 1} \neq \delta^{a_i - 1}$.

From Equation (13) and Figure 3, it can be seen that the derivative of the fal function at the piecewise point is not continuous, and there is an abrupt change at $\pm\delta$, which does not have good continuity and smoothness, resulting in the estimated disturbance value being insufficiently smooth, which in turn may lead to the phenomenon of jitter in the control input. To solve this problem, and simultaneously guaranteeing the characteristics of small gain at large error and large gain at small error, a novel continuous nonlinear function named Fal, as shown in Equation (14), is proposed to replace the traditional piecewise function:

$$\begin{aligned} Fal_i(e) &= \lambda_i |\mathrm{arsh}(e)|^{a_i} \arctan(\gamma_i e) \\ &= \lambda_i \left| \ln(e + \sqrt{e^2 + 1}) \right|^{a_i} \arctan(\gamma_i e) \end{aligned} \tag{14}$$

where λ_i, a_i, and γ_i represent the novel nonlinear function parameters.

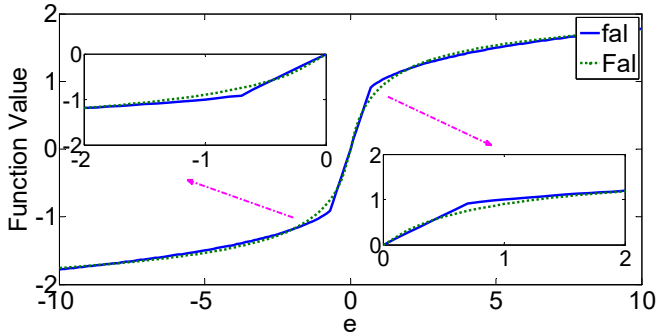

Figure 3. Comparison of nonlinear functions.

It may be useful to consider the case when e > 0, the derivative of the Fal function is obtained, as shown in Equation (15); it is obvious that the derivative of the novel nonlinear function proposed in this paper is also continuous. Therefore, the novel nonlinear function does not have the phenomenon of abrupt changes in function values at piece-

wise points, in contrast to the fal function, which may lead to the jitter phenomenon of disturbance estimation.

$$Fal_i{}'(e) = \lambda_i a_i \frac{\left[\ln(e+\sqrt{e^2+1})\right]^{a_i-1}}{\sqrt{e^2+1}} \arctan(\gamma_i e) + \lambda_i \gamma_i \frac{[\ln(e+\sqrt{e^2+1})]^{a_i}}{\gamma_i{}^2 e^2+1}, e>0 \quad (15)$$

3.2. Stability Analysis of IESO

To analyze the stability of IESO, define the observer error quantity $e = \begin{pmatrix} e_1 & e_2 & e_3 \end{pmatrix}^T$, and let $e_1 = z_1 - x_1$, $e_2 = z_2 - x_2$, $e_3 = z_3 - x_3$, assuming $x_3 = d_0$ is a constant, the error equations (Equations (10) and (11)) can be obtained as

$$\begin{cases} e_1 = z_1 - y \\ \dot{e}_1 = e_2 - \beta_{01} e_1 \\ \dot{e}_2 = e_3 - \beta_{02} Fal_1(e_1) \\ \dot{e}_3 = -\beta_{03} Fal_2(e_1) \end{cases} \quad (16)$$

Rewriting these equations into the form of a state space, we can obtain

$$\dot{e} = -G(e)e \quad (17)$$

where $G(e) = \begin{pmatrix} \beta_{01} & -1 & 0 \\ \beta_{02}\frac{Fal_1(e_1)}{e_1} & 0 & -1 \\ \beta_{03}\frac{Fal_2(e_1)}{e_1} & 0 & 0 \end{pmatrix}$, and also we can see that $\frac{Fal_1(e_1)}{e_1} > 0$, $\frac{Fal_2(e_1)}{e_1} > 0$.

Lemma 1 [25]. If there exists a matrix $H = \begin{pmatrix} h_{11} & h_{12} & h_{13} \\ -h_{12} & h_{22} & h_{23} \\ -h_{13} & -h_{23} & h_{33} \end{pmatrix}$, and the principal diagonal elements of H are positive such that the matrix $HG(e)$ is positive definite symmetric, then the zero solution of the system (17) is Lyapunov asymptotically stable.

According to Lemma 1, it is necessary to construct the matrix H, which satisfies the conditions such that the system is asymptotically stable; calculating $HG(e)$ yields

$$HG(e) = \begin{pmatrix} H_{11} & -h_{11} & -h_{12} \\ H_{21} & h_{12} & -h_{22} \\ H_{31} & h_{13} & h_{23} \end{pmatrix} \quad (18)$$

where $H_{11} = \beta_{01}h_{11} + \beta_{02}\frac{Fal_1(e_1)}{e_1}h_{12} + \beta_{03}\frac{Fal_2(e_1)}{e_1}h_{13}$, $H_{21} = -\beta_{01}h_{12} + \beta_{02}\frac{Fal_1(e_1)}{e_1}h_{22}$ $+\beta_{03}\frac{Fal_2(e_1)}{e_1}h_{23}$, $H_{31} = -\beta_{01}h_{13} - \beta_{02}\frac{Fal_1(e_1)}{e_1}h_{23} + \beta_{03}\frac{Fal_2(e_1)}{e_1}h_{33}$.

According to Equation (18), $HG(e)$ is a positive definite matrix equivalent to

$$\begin{cases} H_{31} = -h_{12}, H_{21} = -h_{11}, h_{13} = -h_{22} \\ \Delta_1 = H_{11} > 0 \\ \Delta_2 = \begin{vmatrix} H_{11} & -h_{11} \\ H_{21} & h_{12} \end{vmatrix} > 0 \\ \Delta_3 = \begin{vmatrix} H_{11} & -h_{11} & -h_{12} \\ H_{21} & h_{12} & -h_{22} \\ H_{31} & h_{13} & h_{23} \end{vmatrix} > 0 \end{cases} \quad (19)$$

Therefore, Lemma 1 is satisfied by constructing a matrix H satisfying Equation (19), such that the zero solution of the system (17) is Lyapunov asymptotically stable. Accordingly, construct the matrix H as in Equation (20) such that $HG(e)$ is a positive definite matrix:

$$H = \begin{pmatrix} 1 & h_{12} & -\varepsilon \\ -h_{12} & \varepsilon & h_{23} \\ \varepsilon & -h_{23} & \varepsilon \end{pmatrix} \quad (20)$$

where $h_{12} = \frac{\beta_{02}\frac{Fal_1(e_1)}{e_1}}{\beta_{01}\beta_{02}\frac{Fal_1(e_1)}{e_1} - \beta_{03}\frac{Fal_2(e_1)}{e_1}} + \varphi_1$, $h_{23} = \frac{1}{\beta_{01}\beta_{02}\frac{Fal_1(e_1)}{e_1} - \beta_{03}\frac{Fal_2(e_1)}{e_1}} + \varphi_2$, ε is a sufficiently small positive number; φ_1, φ_2 are values that are infinitely close to zero with respect to ε; and $Fal_1(e_1)$, $Fal_2(e_1)$ are determined by the corresponding parameters.

Therefore, the Lyapunov function is defined as

$$\begin{aligned} V &= \int_0^t (HG(e)e, \dot{e})d\tau + C \\ &= \int_0^t \left\{ -(\beta_{01}e_1 - e_2)^2 - \varepsilon(\beta_{02}Fal_1(e_1) - e_3)^2 - \varepsilon(\beta_{03}Fal_2(e_1) + d_0)^2 \right\} d\tau + C \end{aligned} \tag{21}$$

where the integrand is bounded and C is a positive number. It is obvious to choose an appropriate positive number C so that $V > 0$.

The derivative of the Lyapunov function is

$$\dot{V} = -(\beta_{01}e_1 - e_2)^2 - \varepsilon(\beta_{02}Fal_1(e_1) - e_3)^2 - \varepsilon(\beta_{03}Fal_2(e_1) + d_0)^2 \leq 0 \tag{22}$$

Thus, this error system in Equation (17) is asymptotically stable at its equilibrium point.

4. The Path-Tracking Controller Design

For the autonomous vehicle path-tracking problem described in this paper, the path-tracking controller is designed based on the IADRC proposed in Section 3, and the direct yaw moment controller is designed to improve the lateral stability of the vehicle; the whole control system structure is shown in Figure 4. The controller adopts the idea of state tracking control; that is, the actual state of the vehicle tracks the desired driving state, so that the lateral deviation and heading error of the vehicle tend to zero, and the yaw rate tracks the desired value, which guarantees the lateral stability of the vehicle during path tracking.

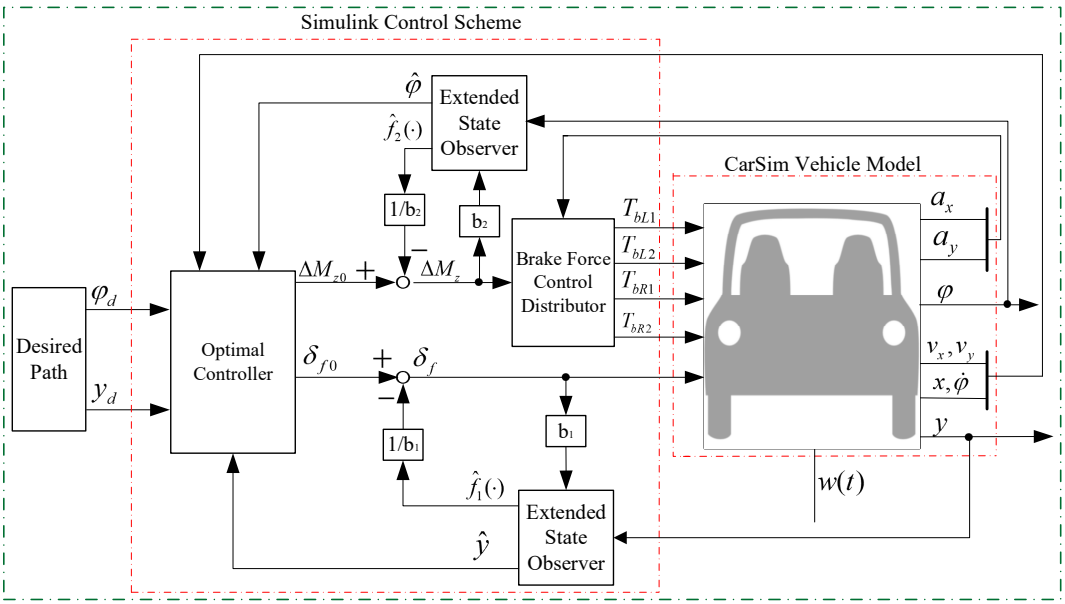

Figure 4. Control scheme structure principle.

The controller takes $x = \left[y_e, \dot{y}_e, \varphi_e, \dot{\varphi}_e\right]^T$ as the controlled variable, based on the linear quadratic regulator method to design the state error compensator to make decisions and output the initial front-wheel steering angle δ_{f0} and the initial external yaw moment ΔM_{z0}. Based on the IESO proposed in Section 3, the disturbance state observer is designed to estimate the total disturbance value in real time, calculate the compensation value, and compensate the front-wheel steering angle and external yaw moment output from the state error compensator, thus obtaining the final front-wheel steering angle δ_f and external yaw moment ΔM_z. To achieve the optimal distribution of the external yaw moment, the braking

force control distributor is designed based on the concept of control allocation (CA), and eventually, the problem of CA can be transformed into the constrained weighted least squares (CWLS) problem.

4.1. IESO for Vehicle Path Following

According to the IESO, the disturbance state observer is designed to estimate the total of the internal and external disturbance acting on the vehicle system. From the 2-DOF dynamics model of the vehicle in Equation (4), Equations (23) and (24) can be obtained:

$$\ddot{y} = f_1(\cdot) + b_1\delta_f \tag{23}$$

where $b_1 = \frac{2C_f}{m}$, $f_1(\cdot) = -\frac{2C_f}{m}\frac{v_y + l_f\dot{\varphi}}{v_x} + \frac{2C_r}{m}\frac{l_r\dot{\varphi} - v_y}{v_x} - v_x\dot{\varphi} + w_1(t)$; $f_1(\cdot)$ denotes the total disturbances on the lateral motion channel, including external disturbance and model uncertainty; and $w_1(t)$ denotes the value of external disturbance:

$$\ddot{\varphi} = f_2(\cdot) + b_2\Delta M_z \tag{24}$$

where $b_2 = \frac{1}{I_z}$, $f_2(\cdot) = \frac{1}{I_z}(l_f F_{yf} - l_r F_{yr}) + w_2(t)$; $f_2(\cdot)$ denotes the total disturbances on the yaw motion channel, which include the external disturbance and model uncertainty; and $w_2(t)$ denotes the value of external disturbance.

Equations (23) and (24) are further rewritten as a second-order system, respectively, which have a single input and single output:

$$\begin{cases} \dot{y}_0 = v_y \\ \dot{v}_y = f_1(\cdot) + b_1\delta_f \\ y_0 = y \end{cases} \tag{25}$$

and

$$\begin{cases} \dot{\varphi}_0 = r \\ \dot{r} = f_2(\cdot) + b_2\Delta M_z \\ \varphi_0 = \varphi \end{cases} \tag{26}$$

Thereby, based on the IESO proposed in Section 3, two extended state observers can be constructed, as shown in Equations (27) and (28):

$$\begin{cases} e_1 = \hat{y} - y_0 \\ \dot{\hat{y}} = \hat{v}_y - \beta_{11}e_1 \\ \dot{\hat{v}}_y = \hat{f}_1(\cdot) - \beta_{12}Fal_{11}(e_1) + b_1\delta_f \\ \dot{\hat{f}}_1(\cdot) = -\beta_{13}Fal_{12}(e_1) \end{cases} \tag{27}$$

and

$$\begin{cases} e_2 = \hat{\varphi} - \varphi_0 \\ \dot{\hat{\varphi}} = \hat{r} - \beta_{21}e_2 \\ \dot{\hat{r}} = \hat{f}_2(\cdot) - \beta_{22}Fal_{21}(e_2) + b_2\Delta M_z \\ \dot{\hat{f}}_2(\cdot) = -\beta_{23}Fal_{22}(e_2) \end{cases} \tag{28}$$

Therefore, according to the content in Section 3, the value of total disturbance estimated by IESO can be derived as

$$\hat{f}(\cdot) = \begin{bmatrix} \hat{f}_1(\cdot) & \hat{f}_2(\cdot) \end{bmatrix}^T \tag{29}$$

4.2. State Error Compensator

The state error compensator is to achieve the state error tending to zero, that is, it makes the lateral deviation and heading error of the vehicle tend to zero. Therefore, the problem of path tracking can be converted to an error minimization problem. In the classic state error compensator in ADRC, there are two kinds, linear and nonlinear; however, their parameter tuning process is more complicated, and the parameter tuning result directly affects the control effect of the controller. Therefore, in this paper, the LQR method is

introduced as the error state compensator, the process of parameter tuning is optimized, and the cost function is defined as

$$J = \frac{1}{2}\int_0^{t_f}\left(x^T Q x + u^T R u\right)dt \tag{30}$$

where $x = \left[y_e, \dot{y}_e, \varphi_e, \dot{\varphi}_e\right]^T$; Q is a semipositive definite matrix that denotes the weight matrix of the controlled variable; and R is a positive definite matrix that denotes the weight matrix of the control input variables.

According to LQR theory, in order to guarantee that the performance index function J is minimized, the control inputs should be as follows:

$$u = -R^{-1}B_0^T P x \tag{31}$$

where P can be obtained by solving the Riccati equation, as follows:

$$A^T P + PA + Q - PB_0 R^{-1}B_0^T P = 0 \tag{32}$$

As a result, the state error compensator outputs the initial front-wheel steering angle and the initial external yaw moment as

$$\left[\begin{array}{cc} \delta_{f0} & \Delta M_{z0} \end{array}\right]^T = -R^{-1}B_0^T P x \tag{33}$$

By compensating the initial output of the state error compensator according to ADRC theory, the final front-wheel steering angle and external yaw moment required for the vehicle path-tracking control are obtained as

$$\left[\begin{array}{cc} \delta_f & \Delta M_z \end{array}\right]^T = -{R_0}^{-1}B_1^T P_1 x - \widetilde{b}\hat{f}(\cdot) \tag{34}$$

where $\widetilde{b} = \left[\begin{array}{cc} 1/b_1 & 0 \\ 0 & 1/b_2 \end{array}\right]$.

4.3. Braking Force Distributor Design

In the previous section, we obtain the external yaw moment by the IADRC controller; the next step is to study how to achieve this external yaw moment. Usually, two forms are available, differential braking and differential driving. Differential braking is chosen in this paper. The CA method can be expressed as follows [26–29]:

$$\begin{cases} v = B_2 u_2 \\ s.t. u_{2\min} \le u_2 \le u_{2\max} \end{cases} \tag{35}$$

where v is the generalized control force, in this paper it is the external yaw moment; B_2 denotes the matrix of control efficiency; u_2 denotes the matrix of control inputs; and $u_{2\max}$, $u_{2\min}$ is the upper and lower limit matrix for the matrix of control inputs.

According to Equation (35), the braking force distribution problem described in this paper can be expressed as the control distributor decides the braking torque of each wheel under the constraint. This is decided by the vehicle and the road, thus achieving differential braking and generating external yaw moment, which can improve the yaw stability of the vehicle. Translated into a mathematical expression, Equation (36) is solved subject to $u_{2\min} \le u_2 \le u_{2\max}$.

$$B_2 u_2 - v = 0 \tag{36}$$

For Equation (36), if there is more than one solution in the constraint range, the solution with the smallest control input is taken, aiming to make the control energy minimum; if there is no solution within the constraint, u_2 is taken under the constraint that $B_2 u_2$ is closest to v. Therefore, the braking force distribution problem in this paper is equivalent to the optimization problem of error minimization and braking force minimization. The two-norm is chosen to evaluate the merit of the solution or the closeness of the solution, so the control allocation problem can be transformed into

$$\begin{cases} \min \omega\|W(u_b - u_d)\|_2^2 + (1-\omega)\|(B_2 u_b - v)\|_2^2 \\ s.t. u_{b\min} \le u_b \le u_{b\max} \end{cases} \tag{37}$$

where ω is the weighting factor for error minimization and control input minimization; u_b is the braking torque of each wheel; and u_d is the desired braking torque, expectation $|u_d|$ is minimal, thus taking $u_d = 0$ here. W is the weight matrix of individual wheel braking forces, and can be defined as

$$W = \mathrm{diag}(w_{L1}, w_{L2}, w_{R1}, w_{R2}) \tag{38}$$

We know that during the movement of the vehicle, the vertical load of each wheel changes, so the maximum braking force that can be achieved by each wheel is different; thus, to obtain a better braking effect, we define the weighting coefficients as follows [12]:

$$\begin{cases} w_{L1} = \frac{mg/4}{F_{zL1}}, w_{R1} = \frac{mg/4}{F_{zR1}} \\ w_{L2} = \frac{mg/4}{F_{zL2}}, w_{R2} = \frac{mg/4}{F_{zR2}} \end{cases} \tag{39}$$

where g is the acceleration of gravity. According to the vehicle dynamics properties, we can obtain

$$\Delta M_z = F_{xbL1}(-\frac{t_{w1}}{2}\cos\delta_f + l_f \sin\delta_f) + F_{xbR1}(\frac{t_{w1}}{2}\cos\delta_f + l_f \sin\delta_f) + (F_{xbR2} - F_{xbL2})\frac{t_{w2}}{2} \tag{40}$$

Thus, the control input matrix of Equation (37) can be expressed as

$$B_2 = \begin{bmatrix} -\frac{t_{w1}}{2}\cos\delta_f + l_f \sin\delta_f & \frac{t_{w1}}{2}\cos\delta_f + l_f \sin\delta_f & -\frac{t_{w1}}{2} & \frac{t_{w1}}{2} \end{bmatrix} \tag{41}$$

Considering

$$\begin{aligned} J &= \omega\|(B_2 u_b - v)\|_2^2 + (1-\omega)\|W(u_b - u_d)\|_2^2 \\ &= \left\| \begin{pmatrix} \sqrt{\omega}B_2 \\ \sqrt{(1-\omega)}W \end{pmatrix} u_b - \begin{pmatrix} \sqrt{\omega}v \\ \sqrt{(1-\omega)}Wu_d \end{pmatrix} \right\|_2^2 \end{aligned} \tag{42}$$

Let $\overline{B}_2 = \begin{pmatrix} \sqrt{\omega}B_2 \\ \sqrt{(1-\omega)}W \end{pmatrix}$, $\overline{v} = \begin{pmatrix} \sqrt{\omega}v \\ \sqrt{(1-\omega)}Wu_d \end{pmatrix}$; thus, the CA problem is transformed into the constrained weighted least squares (CWLS) problem, which can be expressed as

$$u_b = \arg \min_{u_{b\min} \le u_b \le u_{b\max}} \|\overline{B}_2 u_b - \overline{v}\|_2^2 \tag{43}$$

Equation (43) can be solved by the active set method.

However, to solve Equation (43), the brake force constraint should also be defined; it is obvious that the road braking force of the wheel is determined by the vertical load of the wheel and the road adhesion coefficient; thus, in this paper we use an empirical formula to define the upper and lower limits value of the braking force of each wheel. Please refer to [28,29] for details.

5. Results and Discussion

A joint CarSim and Simulink simulation is used to verify the control scheme proposed in this paper, the CarSim/Simulink cosimulation structure diagram is shown in Figure 5. The simulation scenario is a double-lane change maneuver [30], as shown in Equation (44); the desired path and desired heading angle are shown in Figure 6. The simulation speed of the vehicle is set at 70 Km/h and the road adhesion coefficient is set to 1.0. The parameters of autonomous vehicle used in the simulation are listed in Table 1; for more detailed parameters, please refer to the CarSim software for D-Class, SUV model. To fully validate the IESO proposed in this paper, the state error compensator in the ADRC controller in the simulation comparison uses the LQR method.

$$\begin{cases} Y_d(X) = \frac{d_{y1}}{2}[1 + \tanh(p_1)] - \frac{d_{y1}}{2}[1 + \tan(p_2)] \\ \varphi_d = arc\tan\left[d_{y1}(\frac{1}{\cosh(p_1)})^2\right](\frac{1.2}{d_{x1}}) - d_{y2}(\frac{1}{\cosh(p_2)})^2(\frac{1.2}{d_{x2}}) \end{cases} \tag{44}$$

where $d_{x1} = 25$, $d_{x2} = 21.95$, $d_{y1} = 4.05$, $d_{y2} = 5.7$, $p_1 = \frac{2.4}{25}(X - 27.19) - 1.2$, and $p_2 = \frac{2.4}{21.95}(X - 56.46) - 1.2$.

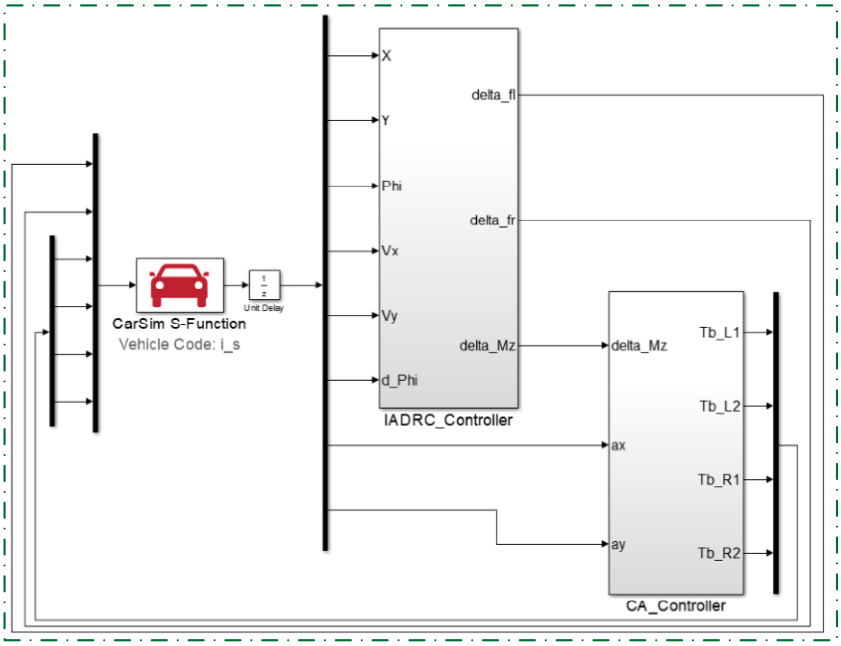

Figure 5. CarSim/Simulink cosimulation structure diagram.

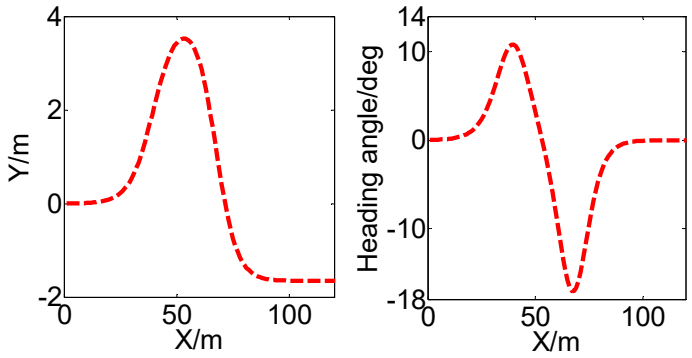

Figure 6. Desired responses of double-lane change maneuver.

Table 1. Parameters of the autonomous vehicle.

Symbol	Parameters	Value and Units
m	Vehicle total mass	1610 kg
I_z	Moment of inertia	2410 kg·m^2
C_f	Cornering stiffness of front wheel	66,900 N/rad
C_r	Cornering stiffness of rear wheel	62,700 N/rad
h_{cg}	Height of the vehicle center of mass	0.65 m
l_f	Front wheel base	1.05 m
l_r	Rear wheel base	1.51 m
t_{w1}	Track width of the front wheels	1.565 m
t_{w2}	Track width of the rear wheels	1.565 m

5.1. Validation of Controller Effectiveness without Disturbance

5.1.1. IADRC Controller Validation

Figures 7 and 8 show the path-tracking result and heading-angle-tracking result; it can be seen that the vehicle controlled by all three controllers are able to follow the desired path precisely. Figures 9 and 10 show the lateral deviation and heading error of the vehicle; we can see that the lateral deviation and heading error of the vehicle are controlled within a smaller range. Moreover, from Table 2, it can be seen that the maximum (absolute value,

same below) and root mean square (RMS) values of lateral deviation and heading error of these three controllers are not very different, among which, the value of IADRC lateral deviation is the smallest with a maximum value of 0.1840 and an RMS value of 0.0593.

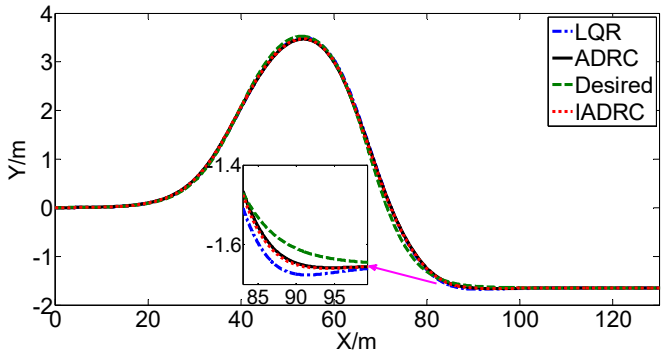

Figure 7. Path-tracking result.

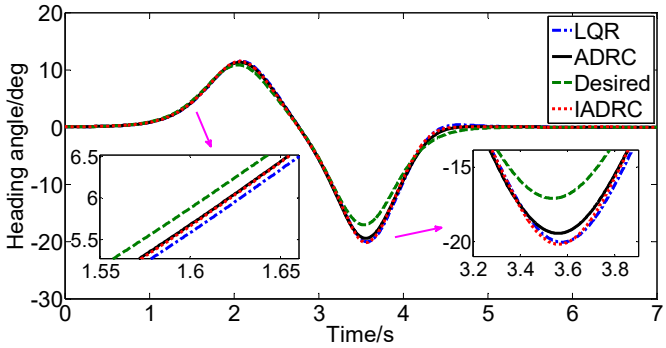

Figure 8. Heading-angle tracking result.

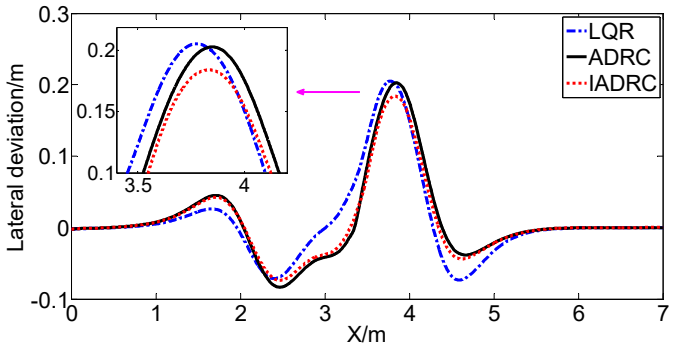

Figure 9. Lateral deviation.

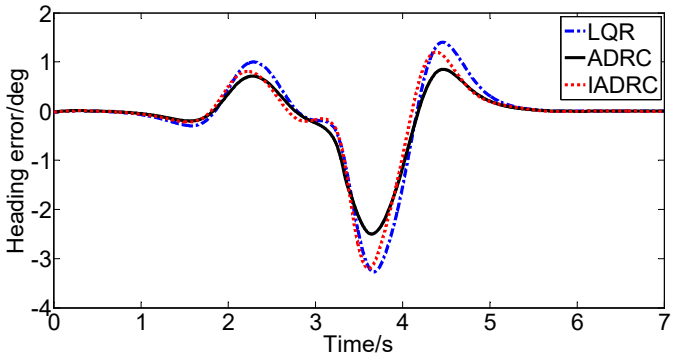

Figure 10. Heading error.

Table 2. Tracking error.

	Lateral Deviation		Heading Error	
	Max	**RMS**	**Max**	**RMS**
LQR	0.2052	0.0602	3.2727	0.9201
ADRC	0.2027	0.0598	2.5001	0.7144
IADRC	0.1840	0.0593	3.2043	0.8360

Figure 11 shows the front-wheel steering angle. It can be seen that the wheel steering angle decided by the LQR controller is small; the front-wheel steering angle decided by the ADRC controller has the phenomenon of jittering from about the fourth to the fifth second—the wheel steering angle input is not smooth; while for the IADRC controller proposed in Section 3, because it uses a nonlinear function with continuity, as shown in Equation (14), the wheel steering angle is smooth and the control input jittering phenomenon is solved.

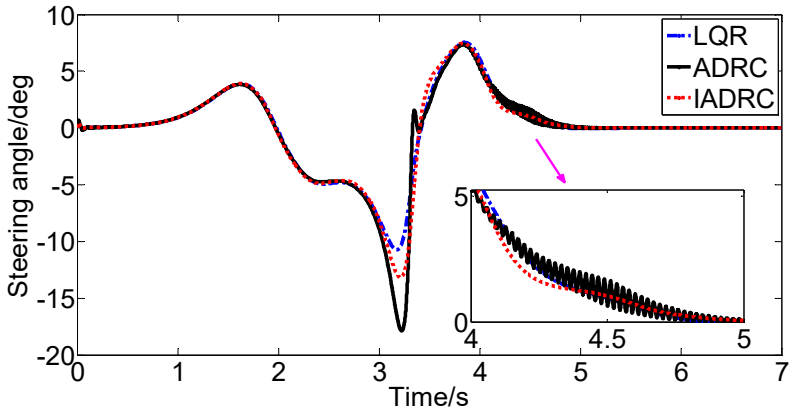

Figure 11. Front-wheel steering angle.

Therefore, according to these simulation results, it can be concluded that the IADRC controller proposed in this paper has higher control performance; the IESO proposed in this paper is able to solve the jittering problem of the control input, and the nonlinear function proposed in this paper is valid.

5.1.2. DYC Controller Validation

The experimental results given above verify the effectiveness of IADRC. To fully verify the performance of the control scheme proposed in this paper, the controller path-tracking accuracy after considering the yaw stability is compared and analyzed through double-lane change maneuver experiments; the performance of braking force distribution based on the CA concept is verified and analyzed.

From Figure 12, it can be seen that the vehicle with and without DYC control both have better path-tracking accuracy; however, from Figure 13, it can be seen that the maximum value of the lateral deviation of the vehicle without DYC control is about 0.20 m, while the same value of the vehicle with DYC control is about 0.15 m; from Figure 14, it can be seen that the heading error of the vehicle is smaller after DYC control is applied. Moreover, Table 3 shows the maximum values and the RMS values of the tracking error for the cases of DYC control and no DYC control. It can be seen that after applying DYC control, the maximum value of lateral deviation is 0.1425 and the RMS value is 0.0456, both of which are smaller than the case without DYC control; similarly, the maximum value of heading angle is 2.6322 and the RMS value is 0.6601, both of which are also lower than the case without DYC control. Therefore, it can be seen that the path-tracking accuracy of the vehicle after applying DYC control is higher than that of the vehicle without DYC control.

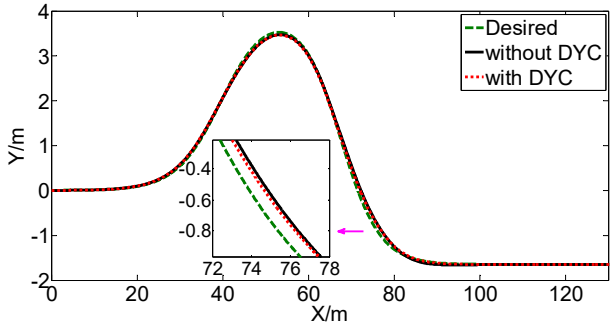

Figure 12. Path-following result.

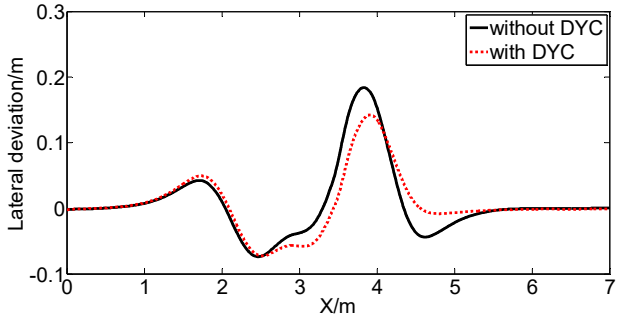

Figure 13. Lateral deviation.

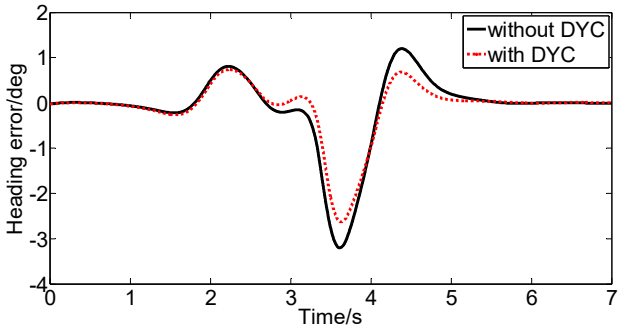

Figure 14. Heading error.

Table 3. Tracking error.

	Lateral Deviation		Heading Error	
	Max	**RMS**	**Max**	**RMS**
IADRC (with DYC)	0.1425	0.0456	2.6322	0.6601
IADRC(without DYC)	0.1840	0.0539	3.2043	0.8360

Figure 15 shows the vehicle yaw rate response, and Figure 16 shows the vehicle side-slip-angle response. It can be seen that the yaw rate of the vehicle can better track the desired value after DYC control is applied, and the deviation of the yaw rate is smaller; the vehicle side-slip angle is also smaller than that of the vehicle without DYC control. Thus, we can conclude that the vehicle has better lateral stability. From Figures 17 and 18, it can be seen that the braking force distributor based on the concept of CA proposed in this paper can fully and optimally coordinate the four wheels to achieve external yaw moment through the form of differential braking; thus, we can conclude that the braking force distributor proposed in this paper is effective.

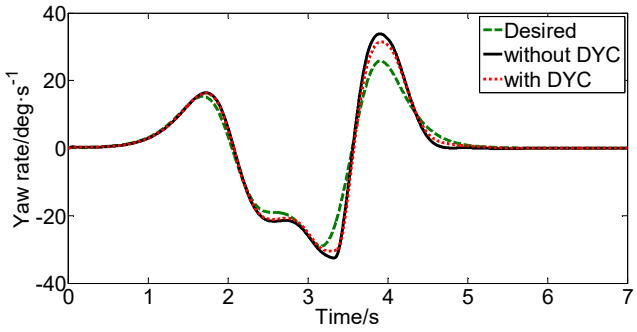

Figure 15. Yaw rate.

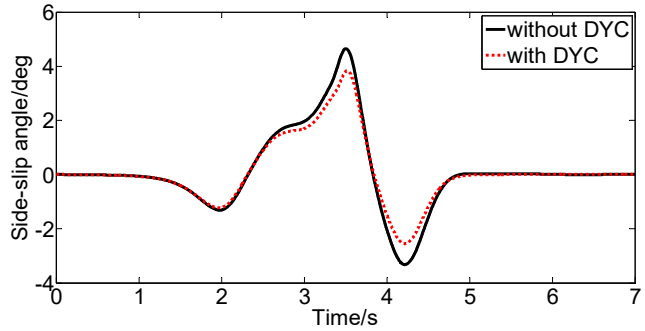

Figure 16. Side-slip angle.

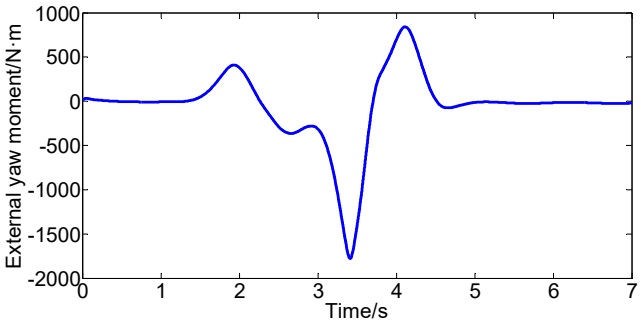

Figure 17. External yaw moment.

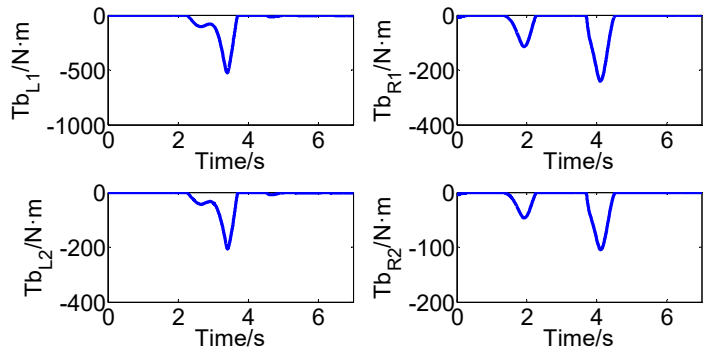

Figure 18. Individual wheel brake torque.

In summary, the IADRC control scheme proposed in this paper has a better path-tracking effect, while the new nonlinear function proposed in this paper instead of the classical piecewise function can solve the problem of variable control input jitter; in the braking force distribution, the braking force distribution scheme with CA method can

optimally coordinate the braking force of each wheel so as to realize direct yaw moment control output from IADRC. Application of DYC control not only improves the path-tracking accuracy, but also improves the yaw stability of the autonomous vehicle.

5.2. Robustness Verification of Resistance to Disturbance

As the main research content of this paper, to verify the robustness of resist disturbance of the IADRC controller, three different kinds of disturbances are applied during the vehicle path tracking, namely a continuous sinusoidal disturbance, a time-changing disturbance, and a step disturbance, and then the control schemes are compared and verified through simulation experiments.

5.2.1. Continuous Sinusoidal Disturbance

Figure 19 shows the vehicle path-tracking result, and Figure 20 shows the vehicle heading-angle tracking result. It can be seen that the control accuracy of the LQR controller deteriorates under the disturbance input, specifically from about the fifth second, the lateral displacement and heading angle of the vehicle both changed obviously with the disturbance. On the contrary, the vehicle with disturbance controlled by the IADRC controller basically reached a steady state similar to the vehicle without disturbance.

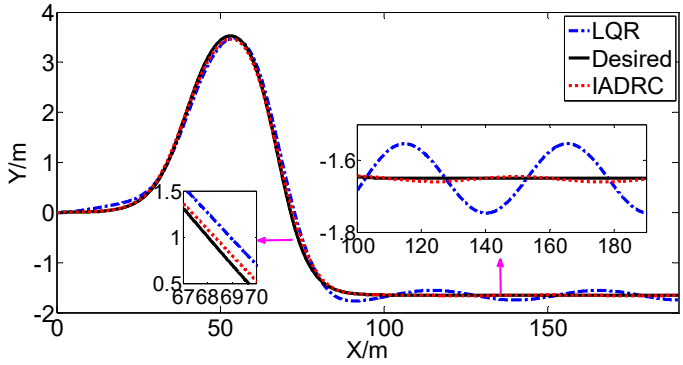

Figure 19. Path-following result.

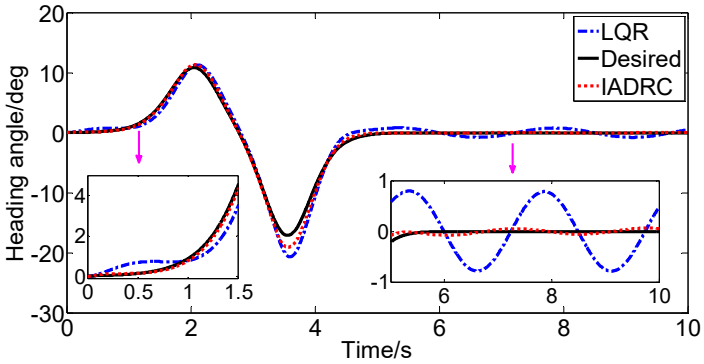

Figure 20. Heading-angle following result.

As can be seen in Figures 21 and 22, the lateral deviation of the vehicle controlled by the LQR controller are larger, from about the fifth second, the vehicle state changes obviously with the disturbance, in which the amplitude of lateral deviation reaches about 0.1 m, and the amplitude of heading error reaches close to 1 deg. On the contrary, the responses of the vehicle controlled by the IADRC controller are smaller; the vehicle with disturbance can also basically reach a steady state from about the fifth second, and the amplitude of lateral deviation is less than 0.01 m, the amplitude of heading error also tends to be close to zero.

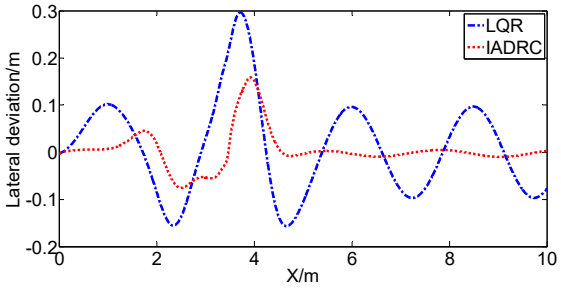

Figure 21. Lateral deviation.

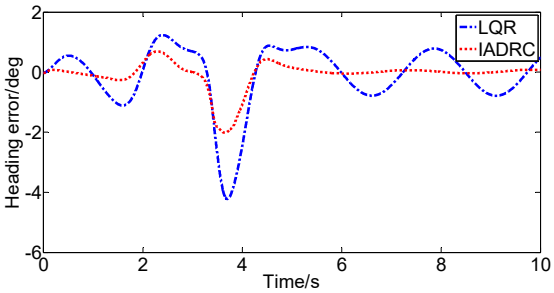

Figure 22. Heading error.

5.2.2. Time-Changing Disturbance

A time-changing disturbance is applied during the path tracking of the autonomous vehicle. As can be seen from Figures 23–26, the path-tracking accuracy of the LQR controller is worse than that of the IADRC controller, with the maximum value of the path-tracking error is about 0.4 m, while the value of the IADRC controller is roughly 0.2 m; similarly, the heading-angle tracking accuracy of the LQR controller is also worse than that of the IADRC, with the maximum value of the heading error exceeding 4 deg, while the value of the IADRC controller is about 2 deg. Therefore, it can be concluded that the IADRC controller is more robust against disturbance than the LQR controller under time-changing disturbances.

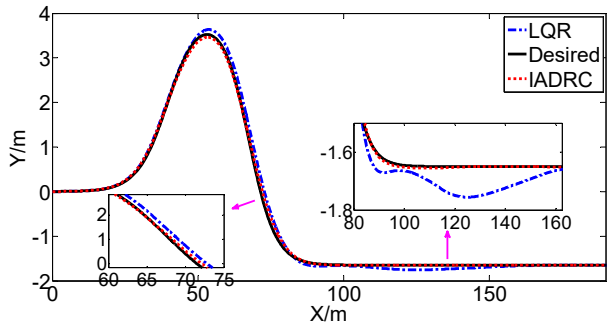

Figure 23. Path-following result.

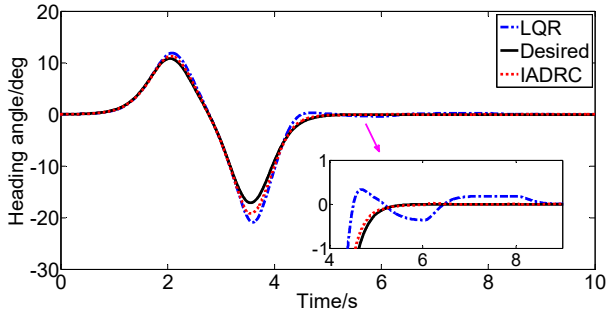

Figure 24. Heading-angle following result.

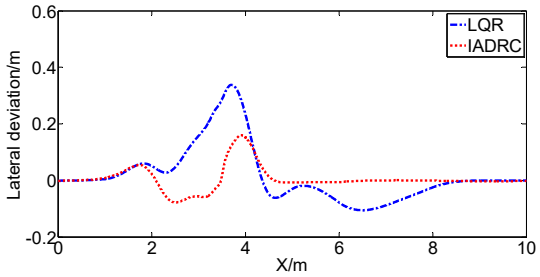

Figure 25. Lateral deviation.

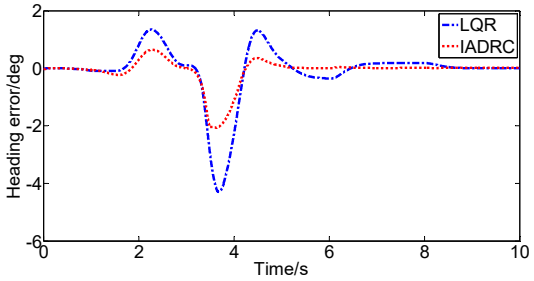

Figure 26. Heading error.

5.2.3. Step Disturbance

During the autonomous vehicle path tracking, a step disturbance is applied starting at the second second and ending at the fifth second. As can be seen from Figures 27–30, the IADRC controller is better able to track the desired path, with the maximum value of the lateral deviation being about 0.16 m, while the value of the LQR is about 0.35 m. Similarly, the vehicle heading-angle tracking accuracy controlled by the IADRC controller exceeds that of the LQR controller, with the maximum value of the heading error is about 2.0 deg, while the value of the LQR controller is about 3.5 deg. Again, it can be seen that the LQR controller's heading error varies more drastically with disturbance than the IADRC controller. Therefore, it can be concluded that the IADRC controller is more robust against disturbance than the LQR controller under step disturbance.

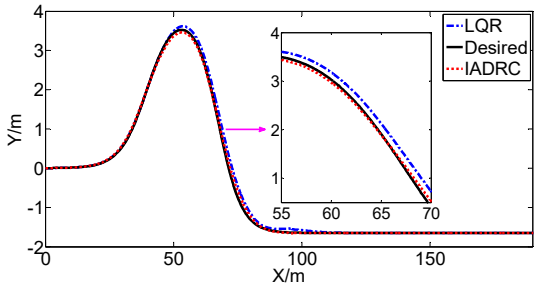

Figure 27. Path-following result.

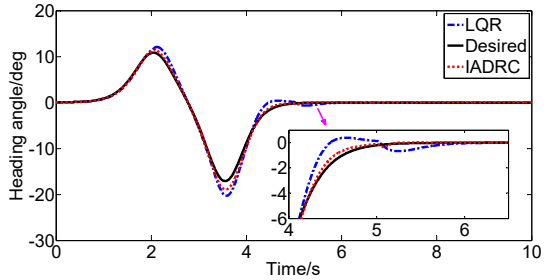

Figure 28. Heading-angle following result.

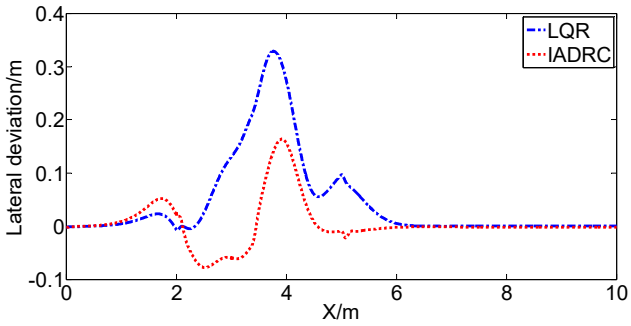

Figure 29. Lateral deviation.

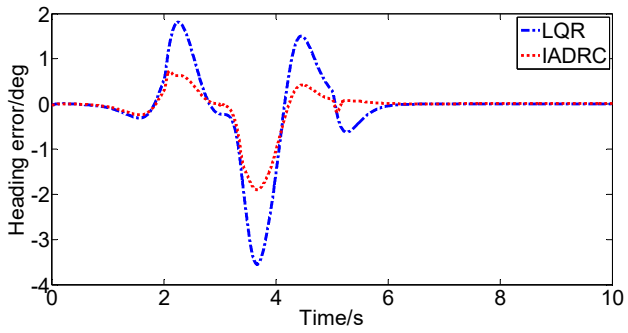

Figure 30. Heading error.

In summary, the autonomous vehicle path-tracking controller designed based on the IADRC method proposed in this paper is effective and feasible in the presence of disturbance. Its path-tracking accuracy and heading-angle tracking accuracy are better than those of the LQR controller, so the antidisturbance robustness of the IADRC controller exceeds that of the LQR controller, which further verifies the effectiveness of the continuous nonlinear function proposed in this paper.

6. Conclusions

In this paper, an improved ADRC control scheme is proposed, based on which an autonomous vehicle path-tracking control scheme is designed, and a DYC controller is designed to improve the lateral stability of the vehicle. Finally, the simulation experimental analysis is carried out in the form of a joint CarSim/Simulink simulation; the results obtained follow:

(1) The proposed IADRC-based autonomous vehicle path-tracking control scheme has better control effect and higher antidisturbance robustness.
(2) The proposed nonlinear continuous function instead of the classical piecewise function can effectively solve the jittering phenomenon of control input, and the IESO designed based on this can accurately estimate the value of disturbance and realize the disturbance compensation in the feedback.
(3) The application of yaw stability control not only improves the yaw stability of the vehicle, but also further improves the path-tracking accuracy. Therefore, simultaneous yaw stability control during the path-tracking process can improve the path-tracking accuracy of the vehicle.
(4) The CA-based braking force distributor can fully coordinate the four wheels to achieve external yaw moment by differential braking, improving the yaw stability of the vehicle.

Author Contributions: Conceptualization, methodology, validation, and software, N.K.; supervision, project administration, and funding acquisition, Y.H.; formal analysis, T.G.; data curation, S.W. All authors have read and agreed to the published version of the manuscript.

Funding: This work was supported in part by the National Key Research and Development Program of China under grant 2021YFE0203600. The authors are greatly thankful for the financial support.

Institutional Review Board Statement: Not applicable.

Informed Consent Statement: Not applicable.

Data Availability Statement: Not applicable.

Acknowledgments: Thanks to all the authors' contribution to this article. Special thanks to Xiujian Yang of Kunming University of Science and Technology.

Conflicts of Interest: The authors declare no conflict of interest.

References

1. Gharavi, H.; Prasad, K.V.; Ioannou, P. Scanning Advanced Automobile Technology. *Proc. IEEE* **2007**, *95*, 328–333. [CrossRef]
2. González, D.; Pérez, J.; Milanés, V.; Nashashibi, F. A Review of Motion Planning Techniques for Automated Vehicles. *IEEE Trans. Intell. Transp. Syst.* **2015**, *17*, 1135–1145. [CrossRef]
3. Yurtsever, E.; Lambert, J.; Carballo, A.; Takeda, K. A Survey of Autonomous Driving: Common Practices and Emerging Technologies. *IEEE Access* **2019**, *8*, 58443–58469. [CrossRef]
4. Badue, C.; Guidolini, R.; Carneiro, R.V.; Azevedo, P.; Cardoso, V.B.; Forechi, A.; Jesus, L.; Berriel, R.; Paixao, T.M.; Mutz, F.; et al. Self-driving cars: A survey. *Expert Syst. Appl.* **2021**, *165*, 113816. [CrossRef]
5. Tan, Q.; Dai, P.; Zhang, Z.; Katupitiya, J. MPC And PSO Based Control Methodology for Path Tracking Of 4WS4WD Vehicles. *Appl. Sci.* **2018**, *8*, 1000. [CrossRef]
6. Yao, Q.; Tian, Y.; Wang, Q.; Wang, S. Control Strategies on Path Tracking for Autonomous Vehicle: State of the art and future challenges. *IEEE Access* **2020**, *8*, 161211–161222. [CrossRef]
7. Lu, H.; Xing, Y.; Zhuo, G.R. Review on Motion Control of Autonomous Vehicles. *J. Mech. Eng.* **2020**, *56*, 127–143. (In Chinese) [CrossRef]
8. Borrelli, F.; Falcone, P.; Keviczky, T.; Asgari, J.; Hrovat, D. MPC-Based Approach to Active Steering FOR Autonomous Vehicle Systems. *Int. J. Veh. Auton. Syst.* **2005**, *3*, 265–291. [CrossRef]
9. Ji, J.; Khajepour, A.; Melek, W.W.; Huang, Y. Path Planning and Tracking for Vehicle Collision Avoidance Based on Model Predictive Control with Multiconstraints. *IEEE Trans. Veh. Technol.* **2016**, *66*, 952–964. [CrossRef]
10. Wang, R.; Yin, G.; Zhuang, J.; Zhang, N.; Chen, J. The Path Tracking of Four-Wheel Steering Autonomous Vehicles via Sliding Mode Control. In Proceedings of the 2016 IEEE Vehicle Power and Propulsion Conference (VPPC) IEEE 2016, Hangzhou, China, 17–20 October 2016; pp. 1–6.
11. Hu, C.; Wang, R.; Yan, F. Integral Sliding Mode-Based Composite Nonlinear Feedback Control for Path Following of Four-Wheel Independently Actuated Autonomous Vehicles. *IEEE Trans. Transp. Electrif.* **2016**, *2*, 221–230. [CrossRef]
12. Chen, T.; Chen, L.; Xu, X.; Cai, Y.; Sun, X. Simultaneous Path Following and Lateral Stability Control Of 4WD-4WS Autonomous Electric Vehicles with Actuator Saturation. *Adv. Eng. Softw.* **2019**, *128*, 46–54. [CrossRef]
13. Hang, P.; Chen, X.; Luo, F. LPV/H∞ Controller Design for Path Tracking of Autonomous Ground Vehicles Through Four-Wheel Steering and Direct Yaw-Moment Control. *Int. J. Automot. Technol.* **2019**, *20*, 679–691. [CrossRef]
14. Mashadi, B.; Ahmadizadeh, P.; Majidi, M.; Mahmoodi-Kaleybar, M. Integrated Robust Controller Design for Vehicle Path Following. *Multibody Syst. Dyn.* **2015**, *33*, 207–228. [CrossRef]
15. Lin, F.; Wang, S.; Zhao, Y.; Cai, Y. Research on Autonomous Vehicle Path Tracking Control Considering Roll Stability. *Proc. Inst. Mech. Eng. Part D J. Automob. Eng.* **2021**, *235*, 199–210. [CrossRef]
16. Hong, S.; Hedrick, J.K. Roll Prediction-Based Optimal Control for Safe Path Following. In Proceedings of the 2015 American Control Conference (ACC), Chicago, IL, USA, 1–3 July 2015; pp. 3261–3266.
17. Chen, T.; Chen, L.; Xu, X.; Cai, Y.; Jiang, H. Integrated Control of Unmanned Distributed Driven Vehicles Path Tracking and Stability. *Autom. Eng.* **2019**, *41*, 1109. (In Chinese)
18. Hiraoka, T.; Nishihara, O.; Kumamoto, H. Automatic Path-Tracking Controller of a Four-Wheel Steering Vehicle. *Veh. Syst. Dyn.* **2009**, *47*, 1205–1227. [CrossRef]
19. Sang, N.; Chen, L. Design of an Active Front Steering System for A Vehicle Using an Active Disturbance Rejection Control Method. *Sci. Prog.* **2019**, *103*, 36850419883565. [CrossRef]
20. Suhail, S.A.; Bazaz, M.A.; Hussain, S. MPC Based Active Disturbance Rejection Control for Automated Steering Control. *Proc. Inst. Mech. Eng. Part D J. Automob. Eng.* **2021**, *235*, 3199–3206. [CrossRef]
21. Xia, Y.; Lin, M.; Zhang, J.; Fu, M.; Li, C.; Li, S.; Yang, Y. Trajectory Planning and Tracking for Four-Wheel Steering Vehicle Based on Differential Flatness And Active Disturbance Rejection Controller. *Int. J. Adapt. Control. Signal Processing* **2021**, *35*, 2214–2244. [CrossRef]
22. Chu, Z.; Wu, C.; Sepehri, N. Automated Steering Controller Design for Vehicle Lane Keeping Combining Linear Active Disturbance Rejection Control And Quantitative Feedback Theory. *Proc. Inst. Mech. Eng. Part I J. SSyst. Control. Eng.* **2018**, *232*, 937–948. [CrossRef]

23. Han, J.Q. Auto Disturbances Rejection Controller and its Applications. *Control. Decis.* **1998**, *13*, 19–23. (In Chinese)
24. Han, J. From PID to active Disturbance Rejection Control. *IEEE Trans. Ind. Electron.* **2009**, *56*, 900–906. [CrossRef]
25. Lozgachev, G.I. On a Method of Construction of Lyapunov Functions. *Autom. Remote Control.* **1998**, *59*, 1365–1369.
26. Varriale, C.; Voskuijl, M. A Control Allocation Approach to Induce the Center of Pressure Position and Shape the Aircraft Transient Response. *Aerosp. Sci. Technol.* **2021**, *119*, 107092. [CrossRef]
27. Wang, J.; Longoria, R.G. Coordinated and Reconfigurable Vehicle Dynamics Control. *IEEE Trans. Control. Syst. Technol.* **2009**, *17*, 723–732. [CrossRef]
28. Yang, X.J. Optimal Reconfiguration Control of the Yaw Stability of the Tractor-Semitrailer Vehicle. *Math. Probl. Eng.* **2012**, *10*, 904–908. [CrossRef]
29. Yang, X.J.; Kang, N.; Liu, M.X.; Zhou, P. Yaw Stability Control for Tractor-semitrailer Combination Based on Optimal Control Allocation Method. *China J. Highw. Transp.* **2013**, *26*, 182–190. (In Chinese)
30. Gong, J.W.; Jiang, Y.; Xu, W. *Model Predictive Control for Self-Driving Vehicles*; Beijing Institute of Technology Press: Beijing, China, 2014; pp. 22–35. (In Chinese)